analytical chemistry

pubs.acs.org/ac Article

Interception Proximity Labeling for Interrogating Cell Efflux Microenvironment

Guyu Wang, Qiang Li, Yuna Guo, Liusheng Chen, Yunyan Yao, Yihong Zhong, Jiahui Sun, Xiaomin Yan, Hongwei Wang, Xiaojian Wang,* Lin Ding,* and Huangxian Ju

Cite This: *Anal. Chem.* 2023, 95, 17798−17807 Read Online

ACCESS | Metrics & More | Article Recommendations | Supporting Information

ABSTRACT: The difficulty in elucidating the microenvironment of extracellular H_2O_2 efflux has led to the lack of a critical extracellular link in studies of the mechanisms of redox signaling pathways. Herein, we mounted horseradish peroxidase (HRP) to glycans expressed globally on the living cell surface and constructed an interception proximity labeling (IPL) platform for H_2O_2 efflux. The release of endogenous H_2O_2 is used as a "physiological switch" for HRP to enable proximity labeling. Using this platform, we visualize the oxidative stress state of tumor cells under the condition of nutrient withdrawal, as well as that of macrophages exposed to nonparticulate stimuli. Furthermore, in combination with a proteomics technique, we identify candidate proteins at the invasion interface between fungal mimics (zymosan) and macrophages by interception labeling of locally accumulated H_2O_2 and confirm that Toll-like receptor 2 binds zymosan in a glycan-dependent manner. The IPL platform has great potential to elucidate the mechanisms underlying biological processes involving redox pathways.

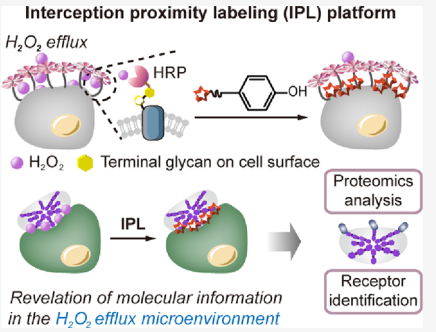

INTRODUCTION

H_2O_2 is a key reactive oxygen species (ROS), and at physiological concentrations, H_2O_2 is a ubiquitous second messenger in the redox signaling pathway.[1] Cells precisely regulate the production, consumption, and extracellular release of H_2O_2, which are essential for maintaining normal physiological processes. For example, cells use NADPH oxidases (Nox) distributed on the plasma membrane to mediate H_2O_2 production and release (Figure 1A) and rely on intracellular peroxidase, glutathione peroxidase, catalase, and myeloperoxidase to consume H_2O_2.[1,2] Detection and labeling of intracellular compartmentalized H_2O_2 have been popular areas of research. Most of the developed sensors consist of an H_2O_2-responsive module and a targeting module,[3−6] and most of the H_2O_2-responsive protein labeling strategies use organic small molecule probes to react with H_2O_2, generating electrophilic reaction intermediates to attack amino acids on neighboring proteins.[7−9]

The extracellular release of H_2O_2, an important process for maintaining cellular H_2O_2 homeostasis, is also of great physiological importance. Plasma membrane is an important platform for the generation, transmission, and regulation of redox signals.[10] H_2O_2 outside the plasma membrane acts as a messenger molecule involved in processes such as intercellular communication,[7] wound healing,[11] and the formation of neutrophil extracellular traps.[12,13] Electrochemical techniques are the classical methods for the detection of extracellular H_2O_2.[14−16] Scanning electrochemical microscopy allows sensitive detection of changes in H_2O_2 levels at the cell surface as well as at various sites outside the surface.[16] As an alternative, a micrometer-scale liquid crystal elastic microsphere, which undergoes concentric-to-radial transfiguration in the presence of H_2O_2, has been exploited to monitor the released H_2O_2 near the plasma membrane.[17] However, existing techniques for the detection of extracellular H_2O_2 cannot dynamically correlate the released H_2O_2 with the heterogeneously distributed biomolecular landscape on the cell membrane. The lack of molecular information in the H_2O_2 efflux microenvironment leads to the absence of key links in the mechanistic study of the redox signaling pathways. Therefore, there is an urgent need to develop methods to visualize and record H_2O_2 efflux events at the plasma membrane by rapidly labeling biomolecules in the H_2O_2 efflux microenvironment in real time.

Extracellular H_2O_2 is characterized by rapid and semi-infinite diffusion. The ideal platform should meet the following three requirements: (1) rapid and specific response to H_2O_2; (2) conversion of H_2O_2 signals into proximity covalent labeling; and (3) broad applicability to a variety of cell types. Inspired by the boom in proximity labeling (PL) technologies,[18−26] we believe that peroxidase is the perfect tool to meet the first two requirements. Peroxidase-dependent proximity labeling tech-

Received: August 29, 2023
Revised: October 31, 2023
Accepted: November 2, 2023
Published: November 17, 2023

https://doi.org/10.1021/acs.analchem.3c03879
Anal. Chem. 2023, 95, 17798−17807

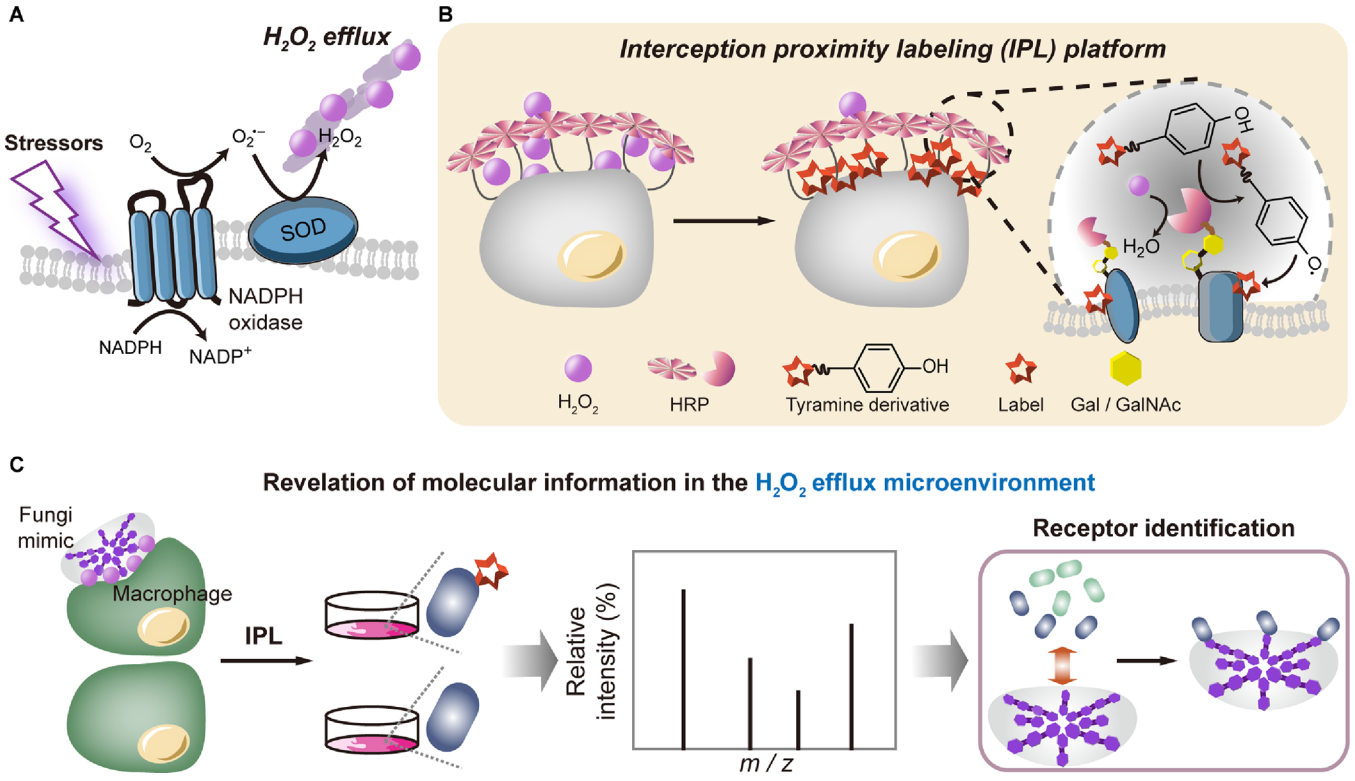

Figure 1. (A) Schematic showing the extracellular release of H_2O_2. Upon exposure to various stressors, cells can generate H_2O_2 efflux via the NADPH oxidase (Nox) pathway. Catalyzed by Nox, electrons from NADPH are transferred to oxygen to form superoxide, which is further disproportionated by superoxide dismutase (SOD) to generate H_2O_2. (B, C) Schematic of the interception proximity labeling principle (B) and its application (C). HRP was mounted to the terminal Gal/GalNAc sites on the living cell surface, which can respond to released H_2O_2 and mediate the labeling of tyramine derivatives to proximal proteins. The combination of the labels with analytical technologies allows the monitoring of extracellular H_2O_2 release and the revelation of molecular information about the microenvironment of H_2O_2 efflux.

nology converts tyramine derivatives into phenoxy radicals with very short lifetimes (<1 ms) and small diffusion radius (<20 nm) in the presence of H_2O_2, allowing the labeling of amino acids (e.g., tyrosine, tryptophan, etc.) adjacent to the enzyme anchor site.[18−25] In combination with quantitative proteomics, this technique has become a powerful tool for dissecting the interaction networks in dynamic biological processes.[20−23] Recently, peroxidase (APEX2 or APEX) has been expressed intracellularly to detect endogenous H_2O_2[27] and to identify the targets of H_2O_2 oxidation by proximity labeling.[28] To meet the third requirement, peroxidase can be mounted to the glycocalyx on the cell surface. This would satisfy the need to respond to H_2O_2 outside the cells and avoid complex genetic manipulation while minimizing the influence on the protein backbone.

Herein, we chose horseradish peroxidase (HRP) as an "H_2O_2 interceptor" and anchored it to the end of glycan chains expressed globally on the surface of living cells to create an interception proximity labeling (IPL) platform for H_2O_2 efflux (Figure 1B). The platform uses the release of endogenous H_2O_2 as a "physiological switch" for HRP to enable spatial proximity labeling, allowing it to be used for real-time monitoring and molecular mechanistic studies of processes related to cellular redox pathways, especially ligand−protein backbone interaction systems. Using tumor cells in a nutrient withdrawal scenario and immune cells in the presence of nonparticulate stimuli as stress models, we demonstrated that the IPL platform can convert the H_2O_2 signal released by cells into a fluorescein or biotin signal covalently attached to the cell membrane, thus enabling the elucidation of the H_2O_2 release pathway and the molecular microenvironment of H_2O_2 efflux. Because of the important role of H_2O_2 release in immune processes, we used H_2O_2 accumulated at the invasion interface between a fungal mimic (zymosan) and a macrophage as a signaling molecule to label proteins associated with phagocytosis (Figure 1C). By combining a quantitative proteomics technique, we further developed an *in situ*, real-time, and high-throughput analytical approach to identify proteins involved in phagocytosis on the macrophage surface and confirmed the role of the recognition receptor Toll-like receptor 2 (Tlr2).

EXPERIMENTAL SECTION

Detailed experimental methods can be found in the Supporting Information.

RESULTS AND DISCUSSION

Design and Characterization of Hydrazide-Modified HRP (HRP-HZ). Since HRP exhibits higher catalytic activity on the cell surface compared to APEX/APEX2[21] and is readily available, we chose HRP to construct the IPL platform. We selected galactose/*N*-acetylgalactosamine (Gal/GalNAc), abundantly expressed on the mammalian cell surface,[29] as the anchor sites for HRP. Gal/GalNAc can be oxidized by galactose oxidase (GAO) to form bioorthogonal aldehyde groups,[30] allowing the coupling with hydrazide-modified HRP (HRP-HZ) to achieve HRP attachment. Such a ligation method is more robust and could not lead to protein clustering when compared to the lectin recognition-based noncovalent installation method for HRP.

https://doi.org/10.1021/acs.analchem.3c03879
Anal. Chem. 2023, 95, 17798−17807

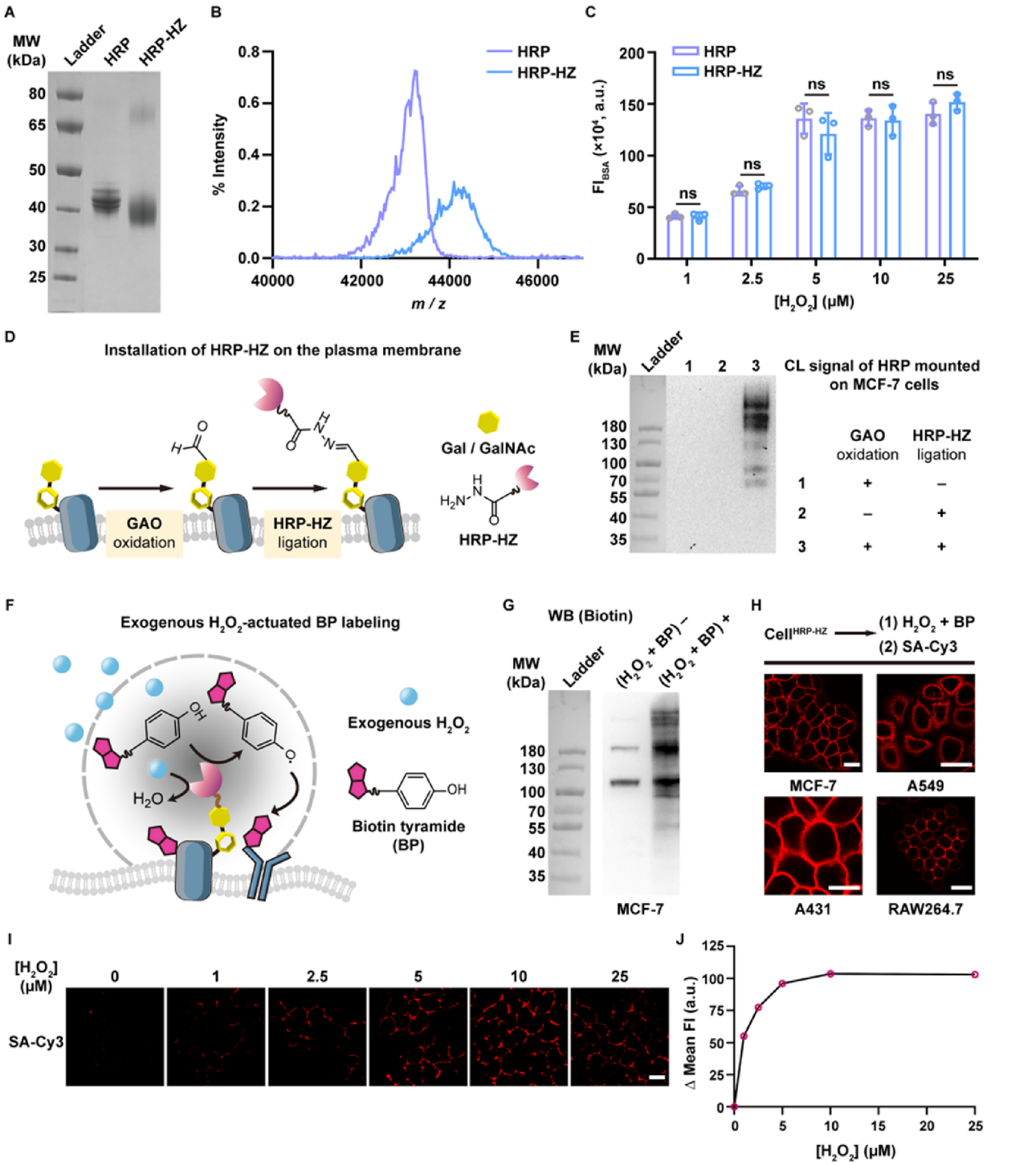

Figure 2. Exogenous H_2O_2-actuated protein labeling by HRP-HZ. (A) SDS-PAGE characterization of HRP-HZ. (B) MALDI-TOF MS characterization of HRP-HZ. (C) In-gel fluorescence analysis of BSA after fluorescein tyramide (FP) labeling catalyzed by HRP-HZ or HRP at different concentrations of H_2O_2. Data are shown as mean ± SD ($n = 3$). ns: no significant difference ($p > 0.05$). (D) Schematic of the installation of HRP-HZ to the plasma membrane. (E) In-gel chemiluminescence (CL) characterization of the catalytic activity of HRP mounted to the MCF-7 cell surface. (F) Schematic of biotin tyramide (BP) labeling catalyzed by cell-mounted HRP in the presence of exogenous H_2O_2. (G) WB analysis of BP-labeled proteins on MCF-7^{HRP-HZ} cells by streptavidin-HRP staining. (H) CLSM imaging of BP labeling on the plasma membrane of different cell types by SA-Cy3 staining. Scale bars: 20 μm. (I) CLSM imaging of BP labeling on MCF-7^{HRP-HZ} cells under different concentrations of exogenous H_2O_2. Scale bar: 20 μm. (J) Mean fluorescence intensity with background subtracted (ΔMean FI) for (I). For each concentration, 20 cells were analyzed by using the LAS-AF-Lite software. Data for (A, B, E, G, H, I, J) are representative of three individual experiments.

To prepare HRP-HZ, we oxidized the glycan chains of HRP[31] with sodium periodate to generate aldehyde groups,[30] followed by a reaction with adipic dihydrazide (ADH) (Figure S1). We demonstrated the successful synthesis of HRP-HZ by SDS-PAGE (Figure 2A) and MALDI-TOF MS (Figure 2B). Using the HRP-catalyzed Amplex Red fluorogenic reaction, we found that 70% of the HRP activity was maintained after ADH modification (Figure S2).

https://doi.org/10.1021/acs.analchem.3c03879
Anal. Chem. 2023, 95, 17798−17807

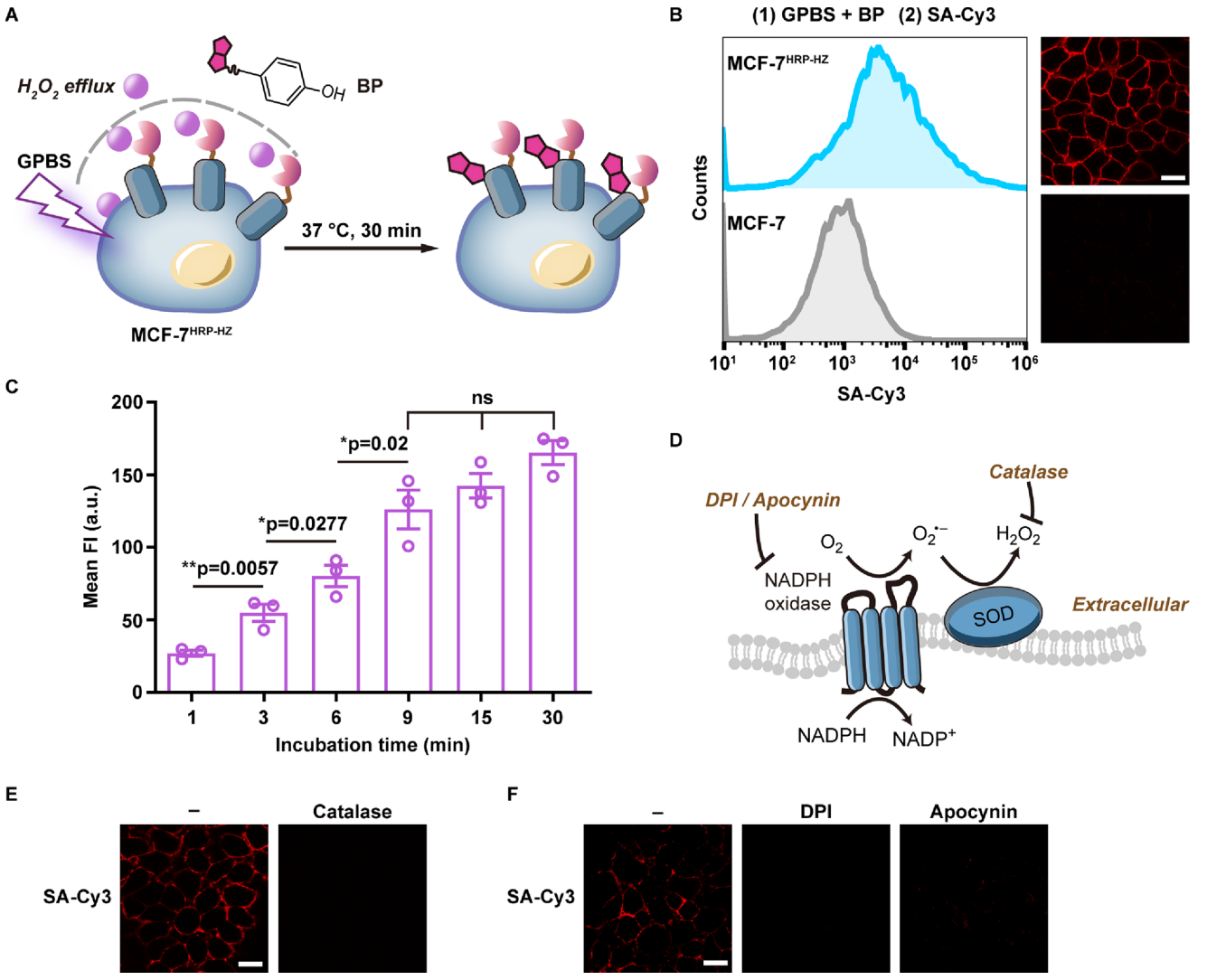

Figure 3. Interception labeling of H_2O_2 efflux from MCF-7 cells actuated by a nutrient withdrawal condition. (A) Illustration of BP labeling on MCF-7^{HRP-HZ} cells upon treatment with GPBS. (B) FCM analysis (left) and CLSM imaging (right) of the BP labeling on MCF-7^{HRP-HZ} cells using SA-Cy3 staining. MCF-7 cells without HRP-HZ mounted were used as a control. Scale bar: 20 μm. (C) Mean FI of SA-Cy3 on MCF-7^{HRP-HZ} cells after incubation with the BP-containing GPBS for different periods and SA-Cy3 staining; 20 cells were analyzed for each time point. Data are shown as mean ± SEM ($n = 3$). *$p < 0.05$, **$p < 0.01$, ns: no significant difference ($p > 0.05$). (D) Illustration of the regulation of the extracellular H_2O_2 level. DPI or apocynin can inhibit Nox, which mediates H_2O_2 production, and catalase can catalyze H_2O_2 decomposition. (E) CLSM imaging of MCF-7^{HRP-HZ} after incubation with BP-containing GPBS in the absence and presence of catalase. Scale bar: 20 μm. (F) CLSM imaging of MCF-7^{HRP-HZ} after pretreatment with Nox inhibitors (DPI, apocynin) and incubation with BP-containing GPBS. Scale bar: 20 μm. Data of (B, E, F) are representative of three individual experiments.

H_2O_2–Responsive Protein Labeling by HRP-HZ. With HRP-HZ in hand, we evaluated the ability of HRP-HZ to label proteins in solution in response to H_2O_2 by adding fluorescein tyramide (FP), HRP-HZ, and exogenous H_2O_2 to BSA (with 20 tyrosine residues, PDB ID: 4F5S). HRP can catalyze the oxidation of FP by H_2O_2 to generate free radical FP$^{\cdot}$, which attacks electron-rich amino acids of neighboring proteins to achieve covalent labeling.[18] The labeling efficiency of HRP-HZ (or HRP, 10 nM) can be conveniently monitored by observing the in-gel fluorescence of BSA-carried FP, which gradually became stronger as the concentration of H_2O_2 increased (0–25 μM), whereas no detectable fluorescence was observed in the absence of H_2O_2 (Figure S3), thus demonstrating that HRP-HZ can respond to H_2O_2 and achieve covalent labeling of FP. The similar labeling ability of HRP-HZ and HRP on BSA indicated that the labeling activity of HRP was well maintained after ADH modification (Figure 2C and Figure S4). When the concentration of HRP-HZ (or HRP) was increased to 10 μM, a negligible fluorescence signal was observed at the HRP-HZ (or HRP) band in the gel, indicating that HRP-HZ (or HRP) would not be labeled by itself (Figure S5). We also confirmed that other common ROS, including $^1O_2$, ·OH, and ClO^-, could not induce FP labeling of BSA, thus demonstrating the response specificity of the reaction (Figure S6).

Mounting HRP-HZ on Cell Surface for Responding to Exogenous H_2O_2. HRP-HZ was then anchored to the cell surface to generate cell^{HRP-HZ} (Figure 2D). We first verified the successful Gal/GalNAc oxidation by GAO (Figure S7). After cell^{HRP-HZ} was lysed and subjected to electrophoretic separation and PVDF membrane transfer, the anchoring of HRP was confirmed by chemiluminescence imaging (Figure 2E). Next, we demonstrated the feasibility of biotin tyramide (BP) labeling

https://doi.org/10.1021/acs.analchem.3c03879
Anal. Chem. 2023, 95, 17798–17807

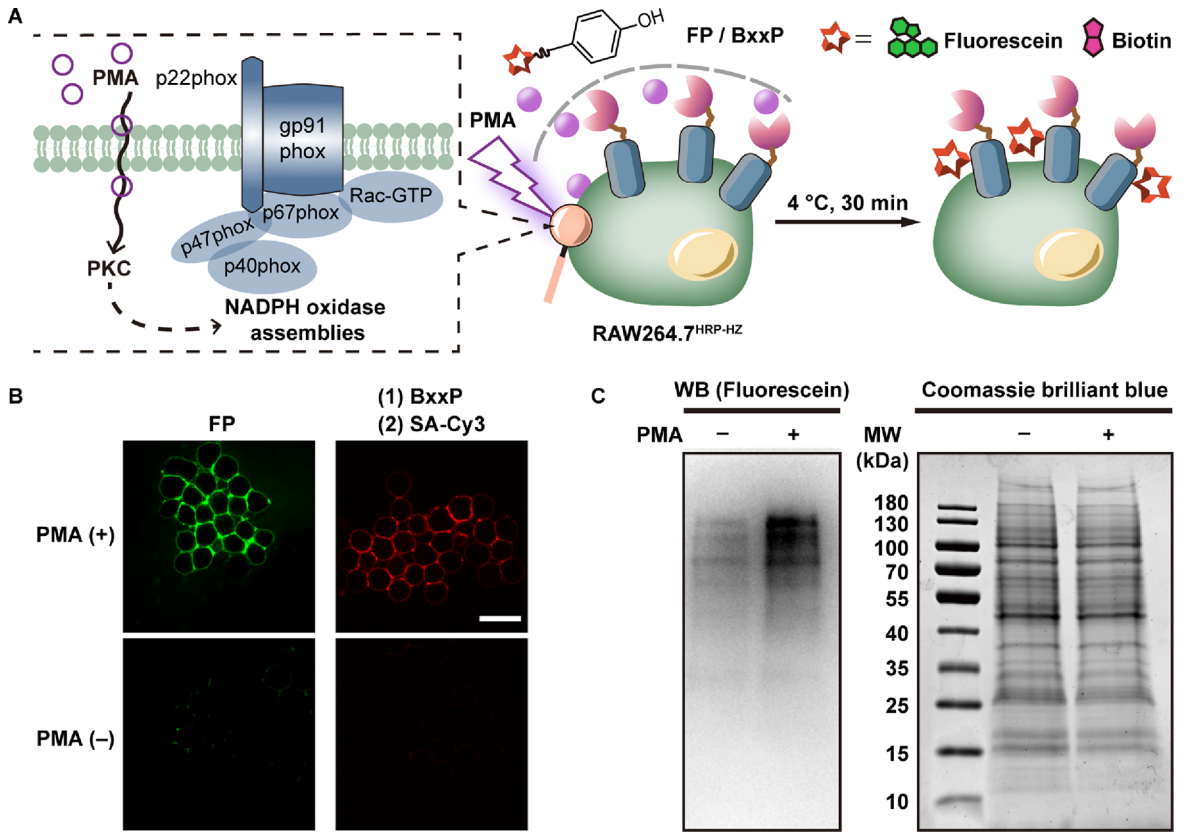

Figure 4. Monitoring of the NADPH oxidase (Nox) assembly mediated H_2O_2 release from RAW264.7 macrophages. (A) Schematic of using the IPL platform to monitor the Nox assembly mediated H_2O_2 release. (B) CLSM imaging of FP and BxxP labeling on RAW264.7^{HRP-HZ} cells with and without PMA treatment. Scale bar: 20 μm. (C) WB analysis of the FP labels on RAW264.7^{HRP-HZ} cells with and without PMA treatment. The right image shows the Coomassie brilliant blue-stained SDS-PAGE gel. Data are representative of three individual experiments.

in the presence of exogenous H_2O_2 using HRP-mounted MCF-7 breast cancer cells as a model by Western blotting (WB) (Figure 2F,G). We also performed streptavidin-Cy3 (SA-Cy3) staining and CLSM imaging on BP-labeled MCF-7^{HRP-HZ}. The bright Cy3 fluorescence on the cell surface indicated successful HRP-HZ-mediated BP labeling (Figure 2H and Figure S8). The cell viability of MCF-7^{HRP-HZ} was similar to that of native cells using two different assay kits (Figure S9). We further installed HRP-HZ on three other cell lines, including lung cancer A549 cells, epidermoid carcinoma A431 cells, and RAW264.7 mouse mononuclear macrophages (Figure 2H and Figure S10). The results showed that the anchoring and labeling operation of HRP-HZ apply to a wide range of cell types. The labeling signal of BP correlated with the H_2O_2 concentration on MCF-7^{HRP-HZ} or A549^{HRP-HZ} (Figure 2I,J, and Figure S11), prompting us to use the developed system to monitor the extracellular release of H_2O_2.

Reporting H_2O_2 Efflux Driven by Nutrient Withdrawal. It is well-known that when cells are starved, metabolic stress is generated and ROS are produced intracellularly.[32−34] The phosphate-buffered saline (PBS) or glucose-containing PBS (GPBS) is a typical "nutrient withdrawal" condition. However, the relationship between PBS incubation and the oxidative stress state of the cells has been largely overlooked. Therefore, we first used the IPL platform to *in situ* monitor the H_2O_2 release proximal to the plasma membrane during GPBS incubation. To minimize the potential effects of GAO oxidation on cells, before exposure to stressors, the cells with HRP-HZ mounted were incubated in a serum-free medium for 2 h to get refreshed. After incubating with GPBS containing BP for 30 min (Figure 3A), the MCF-7^{HRP-HZ} group showed a significant Cy3 fluorescence signal compared to MCF-7 cells (Figure 3B), and the fluorescence intensity increased with the incubation time (Figure 3C and Figure S12), indicating that HRP-HZ mediated the labeling of BP on the cell surface.

To confirm that the labeling was triggered by H_2O_2 released from starved cells, we designed two sets of experiments. (1) The BP labeling signal was substantially reduced by adding catalase (catalyzing the decomposition of H_2O_2, 1000 U/mL) into the system (Figure 3D,E), indicating that the labeling process is triggered by H_2O_2. We further replaced BP with BxxP, a labeling substrate with a biotin moiety but little membrane penetration ability,[20] and increased the concentration of catalase to 15000 U/mL. Compared to the group without catalase, the labeling signal was reduced by about 80% (Figure S13). (2) To confirm that the H_2O_2 reported by the IPL platform was indeed derived from GPBS stimulation, we prepared three groups of cell samples: Cell^{Native} (native cells), Cell^{HRP-HZ} (cells anchored with HRP), and Cell$^{HRP-HZ\ (inactivated)}$ (cells anchored with inactivated HRP) (Figure S14). By measuring H_2O_2 in the supernatants, we confirmed that GPBS incubation could force cells to release H_2O_2 extracellularly (Figure S15). In addition, compared with the Cell^{Native} group, cells in the Cell$^{HRP-HZ\ (inactivated)}$ group did not release more H_2O_2, indicating that the anchoring of HRP-HZ does not trigger H_2O_2 efflux. In the presence of BP, the H_2O_2 concentration in the supernatant of the Cell^{HRP-HZ} group was 69% lower than that of the Cell$^{HRP-HZ\ (inactivated)}$ group,

https://doi.org/10.1021/acs.analchem.3c03879
Anal. Chem. 2023, 95, 17798−17807

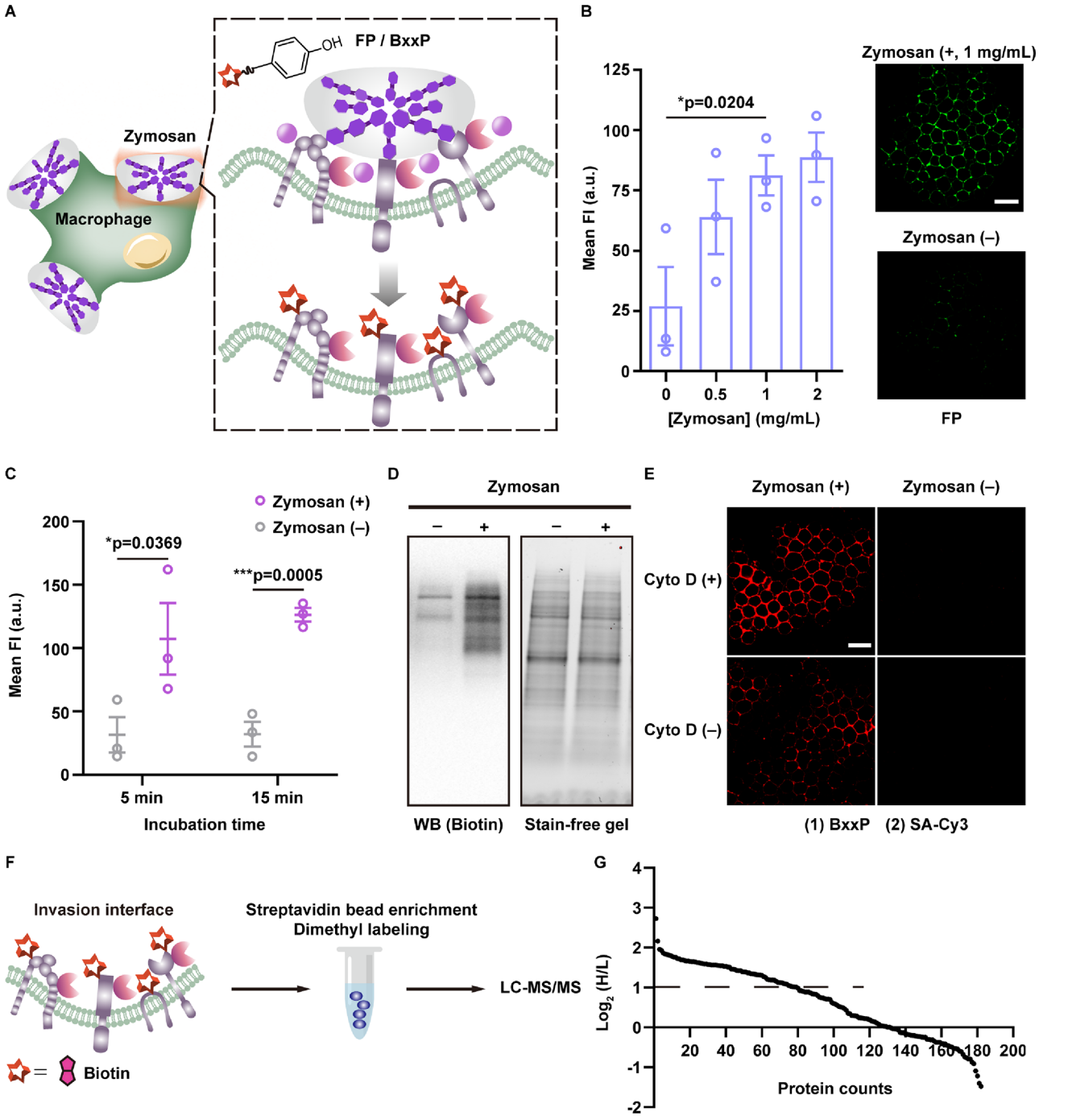

Figure 5. Labeling and identification of proteins at the invasion interface between zymosan and RAW264.7 macrophage. (A) Schematic showing the interception labeling of H_2O_2 efflux at the zymosan invasion interface. (B) Left: mean FI of FP on macrophages after treatment with zymosan at different concentrations. Twenty cells were analyzed for each concentration. Data are shown as mean ± SEM ($n = 3$). *$p < 0.05$; right: representative CLSM images of the FP labels ($n = 3$). Scale bar: 20 μm. (C) Mean FI of SA-Cy3 on macrophages with and without treatment with zymosan for 5 or 15 min using BxxP as the substrate. Twenty cells were analyzed for each condition. Data are shown as mean ± SEM ($n = 3$). *$p < 0.05$, **$p < 0.01$, ***$p < 0.001$. (D) WB analysis of the BxxP-labeled proteins in the whole cell lysates of zymosan (−) and zymosan (+)-treated macrophages using streptavidin-HRP. The stain-free gel image was used as a loading control. (E) CLSM imaging of BxxP labeling on macrophages in different treatment combinations. Scale bar: 20 μm. (F) Workflow for quantitative proteomics using isotope dimethyl labeling. (G) Scatter plot showing the protein counts. Biotinylated proteins in zymosan (+) and zymosan (−) groups were labeled with heavy (H) and light (L) methyl, respectively. The dashed line indicates the threshold for the selection of significantly enriched proteins. Data in (D) are representative of six individual experiments. Data in (E, G) are representative of two individual experiments.

demonstrating that H_2O_2 was indeed consumed during HRP-catalyzed BP labeling (Figure S15).

H_2O_2 production at the cell membrane is closely associated with the assembly of Nox.[35,36] To elucidate the production mechanism of H_2O_2 efflux under the stress of GPBS, MCF-$7^{HRP\text{-}HZ}$ was subjected to treatment with Nox inhibitors (diphenyleneiodonium chloride (DPI) or apocynin) (Figure 3D)[10] before GPBS incubation, and a significant reduction in

https://doi.org/10.1021/acs.analchem.3c03879
Anal. Chem. 2023, 95, 17798−17807

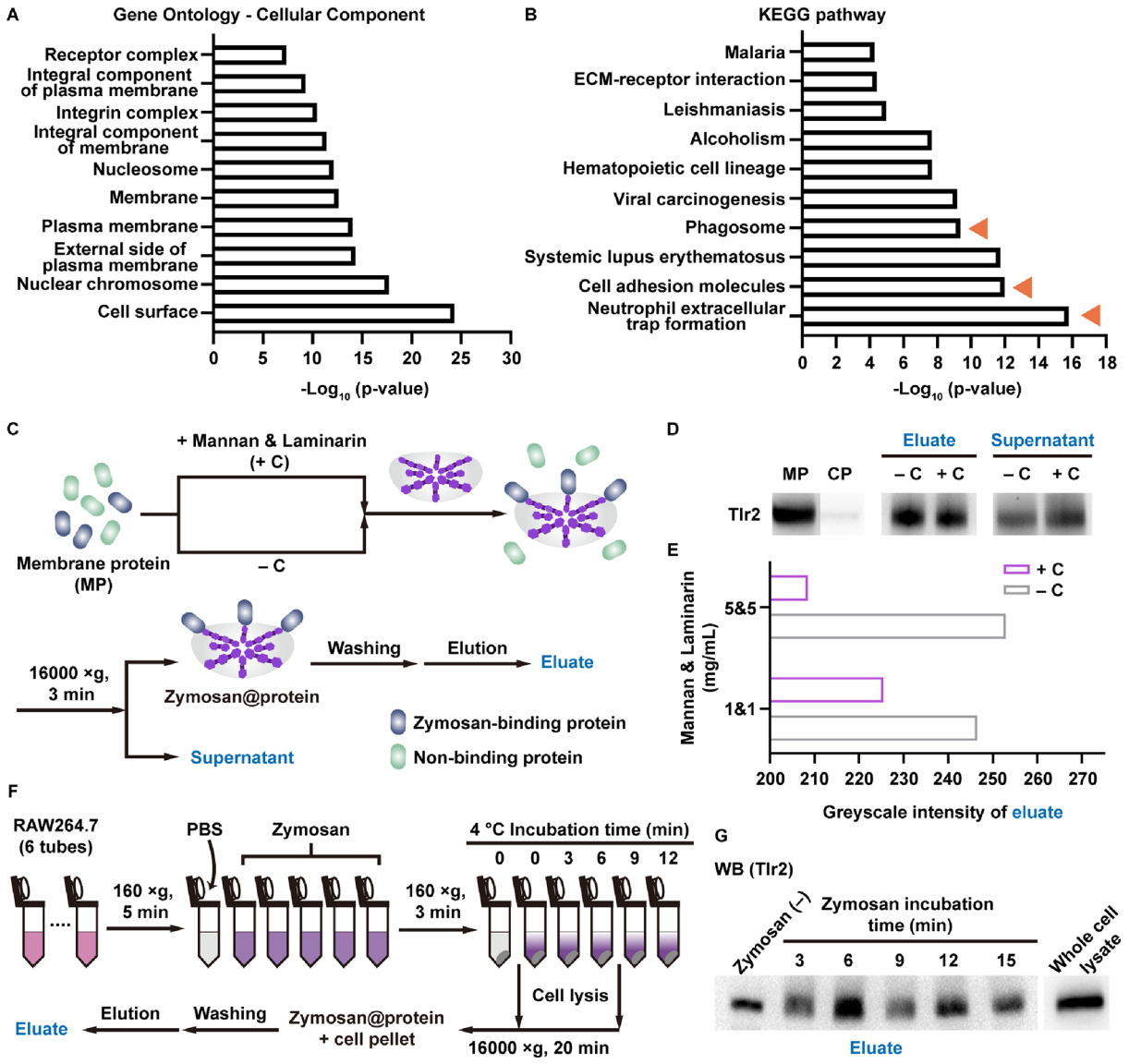

Figure 6. Functional analysis of the proteins labeled at the zymosan invasion interface. (A) Cellular component analysis of the candidate proteins with significant enrichment (listed in Table S1) in Gene Ontology analysis. (B) KEGG pathway analysis of the candidate proteins (listed in Table S1). The pathways associated with phagocytosis are marked with triangles. (C) Schematic of the collection procedure of membrane proteins (MPs) bound to zymosans after *in vitro* incubation. In a control group, mannan and laminarin (C) were added to compete with zymosans for MPs. (D) WB analysis of Tlr2 in different samples. MP: membrane protein, CP: cytosol protein, C: mannan and laminarin competitors. (E) Grayscale intensity of the Tlr2 band in the eluate for the +C and −C groups with different concentrations of mannan and laminarin. (F) Schematic of *in situ* demonstration of the zymosan binding with Tlr2 on RAW264.7 macrophages. (G) WB analysis of Tlr2 in the eluates obtained in (F). Data are representative of two individual experiments.

the BP labeling signal was observed (Figure 3F). This suggests a relationship between GPBS-induced H_2O_2 release and Nox activity and that the IPL platform may indeed reflect the level of H_2O_2 proximal to the cell membrane.

Monitoring of H_2O_2 Released from Macrophages Triggered by Nonparticulate Stimuli. Macrophages normally produce ROS in response to nonparticulate stimulation or phagocytosis.[9,37,38] As mentioned above, the production and release of H_2O_2 involve the assembly of Nox. One of the major modes of assembly is mediated by protein kinase C (PKC). PKC phosphorylates p47phox in the p67phox-p47phox complex in the cytoplasm. The complex transfers to the cell membrane and assembles with the Nox protein to form the Nox assemblies.[36] We used a classical PKC activator, phorbol 12-myristate 13-acetate (PMA), as a nonparticulate stressor to treat RAW264.7 macrophages to mimic Nox assembly in the immune response[39−41] and used the IPL platform to monitor the release of H_2O_2 adjacent to the plasma membrane during this process (Figure 4A).

We first confirmed the successful anchoring of HRP-HZ on cells and the excellent cellular viability of RAW264.7$^{HRP\text{-}HZ}$ (Figures S16 and S17). After treatment with PMA and FP for 30 min, significant FP fluorescence in PMA (+) was observed on the plasma membrane (Figure 4B), indicating the production of H_2O_2 under PMA stimulation. The replacement of FP with BxxP led to a consistent phenomenon, indicating that H_2O_2 consumed by the labeling reaction is indeed present outside the plasma membrane (Figure 4B). We further investigated the covalent labeling of proteins in the H_2O_2 efflux microenvironment by the WB (Figure 4C). The PMA (+) group showed a

https://doi.org/10.1021/acs.analchem.3c03879
Anal. Chem. 2023, 95, 17798−17807

more pronounced blotting signal, and the distribution pattern of labeled proteins was significantly different from the protein pattern in the SDS-PAGE gel, suggesting the successful labeling of proteins in the H_2O_2 efflux microenvironment.

Revealing the Biomolecule Landscape at the Fungal Invasion Interface. Currently, research on receptors mediating pathogen adhesion and phagocytosis mainly relies on the tedious extraction of biological samples,[42,43] resulting in the loss of *in situ* molecular information. Thus, we attempted to address this problem using the IPL platform. Fungal infections threaten the lives of millions of people every year. Fungal cell walls are rich in polysaccharides, among which β-1,3-glucan is the most potent pro-inflammatory and immunogenic polysaccharide. These polysaccharide molecules, as fungi-associated molecular patterns, can be recognized by specific receptors on phagocytes.[44,45] It has been documented that H_2O_2 accumulates at the contact interface between phagocytes and fungi or their mimics.[46−48] Therefore, we speculated that the IPL platform could monitor H_2O_2 (Figure 5A). We chose zymosan as a fungal mimic, which is a particulate polysaccharide (approximately 4 μm in size) and composed of typical glycoforms in the cell wall of yeast such as mannans and β-glucans.[49]

Treatment with 1 mg/mL zymosans for 30 min resulted in a substantial FP labeling signal on the RAW264.7$^{HRP\text{-}HZ}$, which was not due to the adsorption of the zymosan@FP complex (Figure 5B and Figure S18). We changed the labeling reagent to BxxP and found that 5 min of stimulation could generate a statistically significant signal in the zymosan (+) group compared to the zymosan (−) group (Figure 5C and Figure S19). We performed biotin immunoblotting on the two sample groups after 15 min of incubation with zymosan. The zymosan (+) group exhibited stronger biotin labeling and additional protein bands, and the distribution pattern differed from the protein pattern of the SDS-PAGE images (Figure 5D), as well as that of the previous PMA-stimulated group (Figure 4C). This demonstrates that the IPL platform can perform protein proximity labeling in response to H_2O_2 released during the zymosan invasion of macrophages.

We then coupled the IPL platform and cytochalasin D (Cyto D, a phagocytosis inhibitor[50]) to elucidate the mechanism of H_2O_2 release actuated by zymosan invasion. The BxxP labeling signal was significantly enhanced in the Cyto D (+) group compared to that in the Cyto D (−) group (Figure 5E). These data suggest that the release of H_2O_2 should occur earlier than the phagocytosis of zymosan into the cell. Thus, the IPL platform provides an ingenious tool to investigate the mechanism of H_2O_2 efflux in antifungi immunity.

During phagocytosis, discrete receptors expressed on the plasma membrane of phagocytes are capable of recognizing particles and initiating signaling cascades that involve massive reorganization of membrane proteins, remodeling of membrane lipids, and actin cytoskeleton-regulated membrane movement at particle contact sites to form phagocytic cups.[51] We further combined the labels generated by the IPL platform with the quantitative proteomics technique[52] to analyze the proteins involved in the zymosan invasion of macrophages. Biotinylated proteins from zymosan (−) and zymosan (+) treatment of RAW264.7$^{HRP\text{-}HZ}$ (using BxxP as the labeling substrate) were enriched and labeled with light (L) and heavy (H) methyl, respectively, followed by LC-MS/MS analysis (Figure 5F). We identified a total of 183 biotinylated proteins, of which 79 candidate proteins had a $\log_2$ (H/L ratio, fold change) greater than one, indicating these proteins were biotinylated to a significantly higher extent than the others (Figure 5G and Table S1).

Gene ontology (GO) analysis revealed that the functional proteins located on the cell surface were the most highly enriched (Figure 6A). Based on the KEGG pathway analysis, we found a high enrichment of proteins from pathways involved in phagocytosis. These pathways include neutrophil extracellular trap formation, cell adhesion molecules, and phagosome (Figure 6B). Receptors that recognize foreign particles on phagocytes mainly include opsonic phagocytic receptors and pattern-recognition receptors (PRRs).[51,53,54] Among the 79 candidate proteins (Table S1), several significantly enriched biotinylated proteins associated with phagocytosis are summarized in Table 1: for the class of opsonic phagocytic receptors, Fcgr1 (Fc receptor), $\alpha_M\beta_2$ (complement receptor), and $\alpha_5\beta_1$ were found to be significantly enriched; for the class of PRRs, C-type lectins (Clec12a), Toll-like receptors (Tlr2, Tlr1), scavenger receptors (Cd36), and Cd14 were detected. Among them, $\alpha_M\beta_2$ and Toll-like receptor 2 (Tlr2) have been reported as recognition receptors of zymosan.[55−58] In addition to these two classes, we also detected some adhesion-related proteins, phosphorylation-regulating proteins that may serve as oxidized targets for H_2O_2 in the redox signaling pathways and proteins that regulate membrane motility.

Table 1. List of Significantly Enriched Biotinylated Proteins Associated with Phagocytosis

category	biotinylated protein
opsonic phagocytic receptor	Fcgr1, $\alpha_M\beta_2$, $\alpha_5\beta_1$
pattern-recognition receptor	Clec12a, Tlr2, Tlr1, Cd36, Cd14
adhesion-related protein	Icam1, Icam2, Cadm1
phosphorylation-regulating protein	Ptprc, Ptprj
cytoskeleton protein	Tubb5, Tuba1b, Tuba1c, Tuba1a, Tuba3a

Tlr2 is a classical pattern recognition receptor, the signaling pathways of which are closely associated with inflammatory responses in innate immune defense.[58] We extracted the membrane proteins of RAW264.7 macrophages, incubated them with zymosan in vitro, and analyzed the proteins in the eluates by WB (Figure 6C). We found that Tlr2 was predominantly located on the cell membrane and the presence of Tlr2 was identified in the eluate (Figure 6D). To demonstrate that polysaccharide recognition is involved in the interaction, we preincubated the membrane proteins with mannan and laminarin (β-glucan), followed by zymosan incubation. The amount of Tlr2 decreased in the eluate and increased in the supernatant (Figure 6D). The effect of competition depended on the concentration of the added polysaccharides (Figure 6E), suggesting that Tlr2 may interact with zymosan based on polysaccharide recognition. We further demonstrated the recognition of zymosan by Tlr2 on macrophages *in situ*. Cells were incubated with zymosan for different periods and then lysed, and the precipitates were eluted and analyzed by WB (Figure 6F,G). The abundance of Tlr2 in the 6 min incubation eluate was significantly higher than that in the zymosan (−) eluate, suggesting the binding of zymosan to Tlr2 on the cell surface, whereas the signal of Tlr2 decreased with incubation time increasing, presumably due to the uptake of zymosan into cells and the dissociation between zymosan and Tlr2 (Figure 6G). These data demonstrate that our proposed IPL platform provides a powerful research tool to unravel the mechanisms of

https://doi.org/10.1021/acs.analchem.3c03879
Anal. Chem. 2023, 95, 17798−17807

biological processes involving redox pathways at the molecular level.

CONCLUSIONS

We developed an IPL platform for H_2O_2 efflux by anchoring HRP at the end of the glycan chains on the surface of living cells. The IPL platform intercepts H_2O_2 present in the semidiffusive environment outside the plasma membrane and converts it into covalent labels on proximal proteins. By coupling IPL with fluorescence imaging, blot analysis, or mass spectrometry techniques, we obtained information about the dynamic microenvironment of H_2O_2 efflux under various stressors (nutrient withdrawal, pathogen invasion). We found that buffer systems routinely used for in vitro cellular experiments resulted in the accumulation of H_2O_2 neighboring the plasma membrane, suggesting that researchers need to consider the contribution of H_2O_2 efflux when analyzing the research results. We further applied our platform to study immune-related H_2O_2 release from macrophages. First, we monitored the release of H_2O_2 during the assembly process of Nox driven by a nonparticulate stimulus. Second, using zymosan invasion of macrophages as an antifungal immune model, we intercepted and labeled the H_2O_2 accumulating at the macrophage-zymosan invasion interface for proteomic identification of candidate proteins involved in the antifungal immune. We also confirmed Tlr2 as the recognition receptor of zymosan. This is the first time that proximity labeling technology has been designed to study the H_2O_2 efflux microenvironment of cells. The use of glycan chains on the cell surface to covalently anchor peroxidases represents a conceptual innovation for deploying the peroxidase-based proximity labeling platform. In the future, peroxidase can also be anchored to the inner leaflet of the plasma membrane by using liposomal fusion-based transport strategies,[59,60] providing research tools to study the H_2O_2-mediated phosphorylation modification of inner leaflet proteins. In addition, we hope to apply the IPL platform to real pathogen invasion processes to interrogate molecular recognition and interaction. In conclusion, our work has inspired new perspectives to study cellular oxidative stress state from outside the cell, providing a powerful tool to understand the mechanisms of biological processes involving redox pathways and promisingly to complement pro-inflammatory and immunological studies based on cytokine assays.[61] The results obtained lay the foundation for the design of drugs and vaccines against pathogenic infections at the molecular level.

ASSOCIATED CONTENT

Supporting Information

The Supporting Information is available free of charge at https://pubs.acs.org/doi/10.1021/acs.analchem.3c03879.

Experimental methods, supplementary figures, table, and references (PDF)

AUTHOR INFORMATION

Corresponding Authors

Xiaojian Wang − *Institute of Advanced Synthesis, School of Chemistry and Molecular Engineering, Nanjing Tech University, Nanjing 211816, China;* orcid.org/0000-0002-1502-8781; Email: ias_xjwang@njtech.edu.cn

Lin Ding − *State Key Laboratory of Analytical Chemistry for Life Science, School of Chemistry and Chemical Engineering and Chemistry and Biomedicine Innovation Center (ChemBIC), Nanjing University, Nanjing 210023, China;* orcid.org/0000-0001-5381-3484; Email: dinglin@nju.edu.cn

Authors

Guyu Wang − *State Key Laboratory of Analytical Chemistry for Life Science, School of Chemistry and Chemical Engineering, Nanjing University, Nanjing 210023, China*

Qiang Li − *State Key Laboratory of Analytical Chemistry for Life Science, School of Chemistry and Chemical Engineering, Nanjing University, Nanjing 210023, China*

Yuna Guo − *State Key Laboratory of Analytical Chemistry for Life Science, School of Chemistry and Chemical Engineering, Nanjing University, Nanjing 210023, China;* orcid.org/0009-0006-7828-0884

Liusheng Chen − *State Key Laboratory of Analytical Chemistry for Life Science, School of Chemistry and Chemical Engineering, Nanjing University, Nanjing 210023, China*

Yunyan Yao − *State Key Laboratory of Analytical Chemistry for Life Science, School of Chemistry and Chemical Engineering, Nanjing University, Nanjing 210023, China*

Yihong Zhong − *State Key Laboratory of Analytical Chemistry for Life Science, School of Chemistry and Chemical Engineering, Nanjing University, Nanjing 210023, China*

Jiahui Sun − *State Key Laboratory of Analytical Chemistry for Life Science, School of Chemistry and Chemical Engineering, Nanjing University, Nanjing 210023, China*

Xiaomin Yan − *State Key Laboratory of Analytical Chemistry for Life Science, School of Chemistry and Chemical Engineering, Nanjing University, Nanjing 210023, China*

Hongwei Wang − *State Key Laboratory of Analytical Chemistry for Life Science, School of Chemistry and Chemical Engineering, Nanjing University, Nanjing 210023, China; Jiangsu Key Laboratory of Molecular Medicine, Medical School, Nanjing University, Nanjing 210093, China*

Huangxian Ju − *State Key Laboratory of Analytical Chemistry for Life Science, School of Chemistry and Chemical Engineering, Nanjing University, Nanjing 210023, China;* orcid.org/0000-0002-6741-5302

Complete contact information is available at: https://pubs.acs.org/10.1021/acs.analchem.3c03879

Author Contributions

G.W. and L.D. conceived the idea. G.W., Q.L., Y.G., and L.C. designed and performed the IPL experiments. Y.Y. and Y.Z. performed the FCM analysis. J.S. performed MALDI-TOF MS characterization. H.W., H.J., X.W., and L.D. supervised the study. G.W., X.Y., and L.D. drafted the manuscript. All authors have given approval to the final version of the manuscript.

Notes

The authors declare no competing financial interest.

ACKNOWLEDGMENTS

We gratefully acknowledge support from the National Natural Science Foundation of China (21974067, 22274073), Fundamental Research Funds for the Central Universities (020514380309, 021414380502, 2022300324), and the State Key Laboratory of Analytical Chemistry for Life Science (5431ZZXM2305, 5431ZZXM2204).

REFERENCES

(1) Sies, H.; Jones, D. P. *Nat. Rev. Mol. Cell Biol.* **2020**, *21*, 363−383.
(2) Dickinson, B. C.; Chang, C. J. *Nat. Chem. Biol.* **2011**, *7*, 504−511.

(3) Abo, M.; Minakami, R.; Miyano, K.; Kamiya, M.; Nagano, T.; Urano, Y.; Sumimoto, H. *Anal. Chem.* **2014**, *86*, 5983−5990.
(4) Srikun, D.; Albers, A. E.; Nam, C. I.; Iavarone, A. T.; Chang, C. J. *J. Am. Chem. Soc.* **2010**, *132*, 4455−4465.
(5) Wu, Z.; Liu, M.; Liu, Z.; Tian, Y. *J. Am. Chem. Soc.* **2020**, *142*, 7532−7541.
(6) Belousov, V. V.; Fradkov, A. F.; Lukyanov, K. A.; Staroverov, D. B.; Shakhbazov, K. S.; Terskikh, A. V.; Lukyanov, S. *Nat. Methods* **2006**, *3*, 281−286.
(7) Iwashita, H.; Castillo, E.; Messina, M. S.; Swanson, R. A.; Chang, C. J. *Proc. Natl. Acad. Sci. U.S.A.* **2021**, *118*, No. e2018513118.
(8) Yik-Sham Chung, C.; Timblin, G. A.; Saijo, K.; Chang, C. J. *J. Am. Chem. Soc.* **2018**, *140*, 6109−6121.
(9) Zhu, H.; Tamura, T.; Fujisawa, A.; Nishikawa, Y.; Cheng, R.; Takato, M.; Hamachi, I. *J. Am. Chem. Soc.* **2020**, *142*, 15711−15721.
(10) Nordzieke, D. E.; Medrano-Fernandez, I. *Antioxidants* **2018**, *7*, 168.
(11) Niethammer, P.; Grabher, C.; Look, A. T.; Mitchison, T. J. *Nature* **2009**, *459*, 996−999.
(12) Brinkmann, V.; Reichard, U.; Goosmann, C.; Fauler, B.; Uhlemann, Y.; Weiss, D. S.; Weinrauch, Y.; Zychlinsky, A. *Science* **2004**, *303*, 1532−1535.
(13) Kenny, E. F.; Herzig, A.; Krüger, R.; Muth, A.; Mondal, S.; Thompson, P. R.; Brinkmann, V.; Bernuth, H. v.; Zychlinsky, A. *eLife* **2017**, *6*, No. e24437.
(14) Gulaboski, R.; Mirčeski, V.; Kappl, R.; Hoth, M.; Bozem, M. *J. Electrochem. Soc.* **2019**, *166*, G82−G101.
(15) Ahmad, T.; Iqbal, A.; Halim, S. A.; Uddin, J.; Khan, A.; El Deeb, S.; Al-Harrasi, A. *Nanomaterials* **2022**, *12*, 1475.
(16) Bozem, M.; Knapp, P.; Mirceski, V.; Slowik, E. J.; Bogeski, I.; Kappl, R.; Heinemann, C.; Hoth, M. *Antioxid. Redox Sign.* **2018**, *29*, 501−517.
(17) Li, W.; Khan, M.; Lin, L.; Zhang, Q.; Feng, S.; Wu, Z.; Lin, J.-M. *Angew. Chem., Int. Ed.* **2020**, *59*, 9282−9287.
(18) Sunbul, M.; Jaschke, A. *Proximity Labeling: Methods and Protocols*; Humana: Clifton, 2019, *2008*, chapter 1−6.
(19) Kang, M. G.; Rhee, H. W. *Acc. Chem. Res.* **2022**, *55*, 1411−1422.
(20) Li, J.; Han, S.; Li, H.; Udeshi, N. D.; Svinkina, T.; Mani, D. R.; Xu, C.; Guajardo, R.; Xie, Q.; Li, T.; Luginbuhl, D. J.; Wu, B.; McLaughlin, C. N.; Xie, A.; Kaewsapsak, P.; Quake, S. R.; Carr, S. A.; Ting, A. Y.; Luo, L. *Cell* **2020**, *180*, 373−386.
(21) Loh, K. H.; Stawski, P. S.; Draycott, A. S.; Udeshi, N. D.; Lehrman, E. K.; Wilton, D. K.; Svinkina, T.; Deerinck, T. J.; Ellisman, M. H.; Stevens, B.; Carr, S. A.; Ting, A. Y. *Cell* **2016**, *166*, 1295−1307.
(22) Lyu, Z.; Sycks, M. M.; Espinoza, M. F.; Nguyen, K. K.; Montoya, M. R.; Galapate, C. M.; Mei, L.; Genereux, J. C. *ACS Chem. Biol.* **2022**, *17*, 1963−1977.
(23) Perez Verdaguer, M.; Zhang, T.; Surve, S.; Paulo, J. A.; Wallace, C.; Watkins, S. C.; Gygi, S. P.; Sorkin, A. *Cell Rep.* **2022**, *39*, No. 110950.
(24) Qin, W.; Cho, K. F.; Cavanagh, P. E.; Ting, A. Y. *Nat. methods* **2021**, *18*, 133−143.
(25) Zhu, H.; Tamura, T.; Hamachi, I. *Curr. Opin. Chem. Biol.* **2019**, *48*, 1−7.
(26) Hesketh, G. G.; Papazotos, F.; Pawling, J.; Rajendran, D.; Knight, J. D. R.; Martinez, S.; Taipale, M.; Schramek, D.; Dennis, J. W.; Gingras, A.-C. *Science* **2020**, *370*, 351−356.
(27) Mishra, P. K.; Park, I.; Sharma, N.; Yoo, C. M.; Lee, H. Y.; Rhee, H. W. *Anal. Chem.* **2022**, *94*, 14869−14877.
(28) Kisty, E. A.; Falco, J. A.; Weerapana, E. *Cell Chem. Biol.* **2023**, *30*, 321−336.
(29) Liu, Z. L.; Li, J. P.; Chen, M. K.; Wu, M. Y.; Shi, Y. J.; Li, W.; Teijaro, J. R.; Wu, P. *Cell* **2020**, *183*, 1117−1133.
(30) Palaniappan, K. K.; Bertozzi, C. R. *Chem. Rev.* **2016**, *116*, 14277−14306.
(31) Wuhrer, M.; Koeleman, C. A. M.; Hokke, C. H.; Deelder, A. M. *Anal. Chem.* **2005**, *77*, 886−894.
(32) Ye, S.; Hu, J. J.; Yang, D. *Angew. Chem., Int. Ed.* **2018**, *57*, 10173−10177.
(33) Li, L.; Chen, Y.; Gibson, S. B. *Cell. signal.* **2013**, *25*, 50−65.
(34) Lee, I. H.; Kawai, Y.; Fergusson, M. M.; Rovira, I. I.; Bishop, A. J. R.; Motoyama, N.; Cao, L.; Finkel, T. *Science* **2012**, *336*, 225−228.
(35) Holmstrom, K. M.; Finkel, T. *Nat. Rev. Mol. Cell Biol.* **2014**, *15*, 411−421.
(36) Lambeth, J. D. *Nat. Rev. Immunol.* **2004**, *4*, 181−189.
(37) Nathan, C.; Cunningham-Bussel, A. *Nat. Rev. Immunol.* **2013**, *13*, 349−361.
(38) Reth, M. *Nat. Immunol.* **2002**, *3*, 1129−1134.
(39) Ambruso, D. R.; Bolscher, B. G.; Stokman, P. M.; Verhoeven, A. J.; Roos, D. *J. Biol. Chem.* **1990**, *265*, 924−930.
(40) Clark, R. A.; Volpp, B. D.; Leidal, K. G.; Nauseef, W. M. *J. Clin. Invest.* **1990**, *85*, 714−721.
(41) Vilhardt, F.; van Deurs, B. *EMBO J.* **2004**, *23*, 739−748.
(42) Carreras-Gonzalez, A.; Barriales, D.; Palacios, A.; Montesinos-Robledo, M.; Navasa, N.; Azkargorta, M.; Pena-Cearra, A.; Tomas-Cortazar, J.; Escobes, I.; Pascual-Itoiz, M. A.; Hradiska, J.; Kopecky, J.; Gil-Carton, D.; Prados-Rosales, R.; Abecia, L.; Atondo, E.; Martin, I.; Pellon, A.; Elortza, F.; Rodriguez, H.; Anguita, J. *PLOS Pathog.* **2019**, *15*, No. e1008163.
(43) Zoued, A.; Zhang, H.; Zhang, T.; Giorgio, R. T.; Kuehl, C. J.; Fakoya, B.; Sit, B.; Waldor, M. K. *Nat. Chem. Biol.* **2021**, *17*, 1199−1208.
(44) Romani, L. *Nat. Rev. Immunol.* **2011**, *11*, 275−288.
(45) Erwig, L. P.; Gow, N. A. *Nat. Rev. Microbiol.* **2016**, *14*, 163−176.
(46) Ohno, Y.; Hirai, K.; Kanoh, T.; Uchino, H.; Ogawa, K. *Blood* **1982**, *60*, 253−260.
(47) Peskin, A. V.; Khramtsov, A. V.; Morozov, I. A.; Zemskov, V. M.; Zbarsky, I. B. *Exp. Cell Res.* **1984**, *151*, 247−251.
(48) Hirai, K. I.; Moriguchi, K.; Wang, G. Y. *Exp. Cell Res.* **1991**, *194*, 19−27.
(49) Di Carlo, F. J.; Fiore, J. V. *Science* **1958**, *127*, 756−757.
(50) Jang, S.; Ohtani, K.; Fukuoh, A.; Yoshizaki, T.; Fukuda, M.; Motomura, W.; Mori, K.; Fukuzawa, J.; Kitamoto, N.; Yoshida, I.; Suzuki, Y.; Wakamiya, N. *J. Biol. Chem.* **2009**, *284*, 3956−3965.
(51) Flannagan, R. S.; Jaumouille, V.; Grinstein, S. *Annu. Rev. Pathol.* **2012**, *7*, 61−98.
(52) Boersema, P. J.; Raijmakers, R.; Lemeer, S.; Mohammed, S.; Heck, A. J. *Nat. Protoc.* **2009**, *4*, 484−494.
(53) Uribe-Querol, E.; Rosales, C. *Front. Immunol.* **2020**, *11*, 1066.
(54) Rosales, C.; Uribe-Querol, E. *BioMed Res. Int.* **2017**, *2017*, No. 9042851.
(55) Ross, G. D.; Cain, J. A.; Lachmann, P. J. *J. Immunol.* **1985**, *134*, 3307−3315.
(56) Aderem, A.; Ulevitch, R. J. *Nature* **2000**, *406*, 782−787.
(57) Akira, S.; Uematsu, S.; Takeuchi, O. *Cell* **2006**, *124*, 783−801.
(58) Kawai, T.; Akira, S. *Nat. Immunol.* **2010**, *11*, 373−384.
(59) Lin, M.; Chen, Y.; Zhao, S.; Tang, R.; Nie, Z.; Xing, H. *Angew Chem., Int. Ed.* **2022**, *61*, No. e202111647.
(60) Chen, Y.; Wu, T.; Xie, S.; Bai, Y.; Xing, H. *Sci. Adv.* **2023**, *9*, No. eadg2583.
(61) Borriello, F.; Poli, V.; Shrock, E.; Spreafico, R.; Liu, X.; Pishesha, N.; Carpenet, C.; Chou, J.; Di Gioia, M.; McGrath, M. E.; Dillen, C. A.; Barrett, N. A.; Lacanfora, L.; Franco, M. E.; Marongiu, L.; Iwakura, Y.; Pucci, F.; Kruppa, M. D.; Ma, Z.; Lowman, D. W.; Ensley, H. E.; Nanishi, E.; Saito, Y.; O'Meara, T. R.; Seo, H. S.; Dhe-Paganon, S.; Dowling, D. J.; Frieman, M.; Elledge, S. J.; Levy, O.; Irvine, D. J.; Ploegh, H. L.; Williams, D. L.; Zanoni, I. *Cell* **2022**, *185*, 614−629.

https://doi.org/10.1021/acs.analchem.3c03879
Anal. Chem. 2023, 95, 17798−17807